Computers and Electronics in Agriculture 186 (2021) 106186

Contents lists available at ScienceDirect

Computers and Electronics in Agriculture

journal homepage: www.elsevier.com/locate/compag

Original papers

A fast and practical one-dimensional transient model for greenhouse temperature and humidity

R. Liu [a], M. Li [b,c], J.L. Guzmán [a,*], F. Rodríguez [a]

[a] Department of Informatics, ceiA3, CIESOL, Ctra. Sacramento s/n, University of Almería, Almería, Spain
[b] Beijing Research Center for Information Technology in Agriculture, National Engineering Research Center for Information Technology in Agriculture, National Engineering Laboratory for Agri-product Quality Traceability, Meteorological Service Center for Urban Agriculture, China
[c] Meteorological Administration - Ministry of Agriculture and Rural Affairs, Key Laboratory of Agri-informatics, Ministry of Agriculture, Beijing, China

ARTICLE INFO

Keywords:
Controlled-environment simulation
Greenhouse climate
Transient model

ABSTRACT

This paper introduces a new transient greenhouse model which uses a mechanistic method to estimate the temperature and humidity in typical Chinese solar greenhouses. A novel and easy-to-use wall temperature estimation method based on the energy balance was adopted for the environment model rather than using boundary temperature measurements. In this way, the number of model inputs is considerably reduced, and the proposed model is able to predict future greenhouse climate conditions by utilizing only the weather forecast. The model validation was performed in two different greenhouses (each with different sizes and physical parameters, such as the greenhouse volume, the roof and wall areas, the wall materials and so on) on three typical days in 2019 and 2020, and over four consecutive weeks in different seasons during 2016 and 2019 . Promising results were obtained and the model performed well in different operating modes; these included having the vents completely closed, opening the vents, and completely closing the vents in the cold season with an additional thermal insulation blanket covering. The validation results demonstrate that the proposed model can be widely adapted to different sizes of typical Chinese solar greenhouses, as well as to different weather conditions. Thus, the developed model is a flexible and valuable tool that can be used for greenhouse climate simulation, temperature and humidity control, and as a decision-making support system to help manage solar greenhouses.

1. Introduction

Greenhouse modeling is a valuable method for understanding the effects of various parameters that influence cooling/heating demand and for obtaining optimal greenhouse operating conditions; this is of fundamental importance when selecting the greenhouse design parameters and when making management decisions in practical production (Choab et al., 2019).

Different aspects of greenhouse modeling can be evaluated including accuracy, functionality, portability and applicability. Designers choose which features to focus on or ignore depending on the model's purpose, thus an optimal model always matches its advantages with the reason it was developed. Zhang et al. developed an accurate model that involved high-resolution solar radiation equations for a Chinese solar greenhouse, considering the crop-environment interaction and including a detailed 3D tomato canopy model. However, a total running time of approximately 20 h was needed to simulate results for an 8-hour period using an Intel Core I7 CPU and 16 GB RAM (Zhang et al., 2020b). The other type of reliable high-resolution model was developed employing the CFD (Computational Fluid Dynamics) method, which also requires a high computational load (Boulard et al., 2017). Li et al. managed to reduce the computational cost by adopting a POD (Proper Orthogonal Decomposition)-based optimization scheme (Li et al., 2020). However, the performance of the model in transient simulations needs to be further studied. Nevertheless, the above models are excellent tools for understanding the temperature field, the solar radiation field and the other physical phenomena in greenhouses. Zhang et al. studied an unsteady-one-dimensional model for a glass greenhouse assuming that the indoor climate elements were uniform (Zhang et al., 2020a). The model considered the dynamic cover absorbance and transmittance caused by the variation in the sun's position as well as the combined effects of the cover, soil and air, thus making it a comprehensive model for temperature simulation. The developer chose to ignore the heterogeneity, ventilation, humidity, crop-environment interaction,

* Corresponding author.
E-mail addresses: lim@nercita.org.cn (M. Li), joseluis.guzman@ual.es (J.L. Guzmán).

https://doi.org/10.1016/j.compag.2021.106186
Received 12 December 2020; Received in revised form 6 April 2021; Accepted 27 April 2021
Available online 13 May 2021

condensation and so on, but the model is still a valuable tool that helps greenhouse designers determine the energy budget.

In this work, the objective has been to develop a model that can be computed rapidly and is widely applicable. The model can be used as a tool for temperature and humidity prediction and for control, two crucial processes for tackling plant disease in the cultivation taking place in typical Chinese single-slope solar greenhouses (Zhao et al., 2011). Currently, this is the main type of greenhouse used for cold-season vegetable production in northern China, with a total area of 1.96 million ha (Liu et al., 2021) being reported. However, these greenhouses lack standardization in terms of their size, structure and materials; two thirds of them are made of rammed soil walls with greenhouse lengths varying from 50 to 100 m and spans (widths) varying from 7 to 12 m (Guo et al., 2016). This makes it difficult to apply the model to a real greenhouse for the following reasons: the wall heat flux should be simulated on a case-by-case basis rather than by imposing an experimental value; the solar radiation gain varies depending on the structure, its size and the roof materials; and the tightness of the cover has been shown to directly influence the degree of air leakage (infiltration) (Jolliet et al., 1991; Ahamed et al., 2018).

In recent years, a variety of control devices have been applied to Chinese solar greenhouses, such as climate sensors, artificial light, CO_2 enrichment, and fan cooling systems. However, these are still at the small-scale demonstration stage. One of the devices most widely adopted by farmers is the thermal insulation blanket rolling machine; this has reached an application rate of more than 90% in Shandong province, the main protected vegetable production area in China, (Wen et al., 2019). Another common approach adopted by most farmers is to use natural ventilation to cool and dehumidify their crops (Li et al., 2018); this is because of the interaction between the energy cost and market prices, which will continue far into the future. Based on the above situations, the scenario in which this model is applied is a naturally ventilated greenhouse without an additional heat source, but where a thermal insulation blanket is included as a roof cover in the cold season.

Limited humidity simulation models have been developed for Chinese solar greenhouses using a mechanistic method. Quantifying the humidity source term seems to be even more difficult than quantifying the energy budget (due to a lack of standardization); this is because of ubiquitous soil evaporation and plant transpiration. The humidity source coming from plant transpiration has been quantified based on the stomatal resistance of several common cultivars grown in greenhouses (Villarreal-Guerrero et al., 2012). A few predictive humidity models have been designed over the last decade for Chinese solar greenhouses although these have neglected to include evapotranspiration and condensation (Zhang et al., 2019a). Under conditions in which the vents remain closed, the greenhouse humidity increases in the morning due to evapotranspiration from the crop canopy or the soil. With the decrease in temperature after midday, the humidity reduces by condensation or liquidation. In addition, air leakage occurs the entire time. The above mechanisms form the mass budget for greenhouse humidity under closed-vent conditions. Each of the modeling mechanisms is complex, which is why few mechanistic humidity models are applied to real situations.

Several predictive temperature and humidity models based on machine learning methods have been reported (Zou et al., 2017; He and Ma, 2010). Furthermore, various black box models have been developed to simulate temperature and humidity in glass greenhouses using machine learning methods such as neural networks and deep learning techniques (Jung et al., 2020). Black box models can be easily applied to real greenhouses and can predict future climate conditions. However, the data need to be collected and trained independently to make them applicable to different types of greenhouses. For mechanistic or white box models based on physical laws (Righini et al., 2020; Chen et al., 2020), boundary conditions limit the models' functioning. In many cases, real-time wall temperature or heat flux parameters are needed as model inputs (Boulard et al., 2017; Kichah et al., 2012), which makes it impossible to simulate the future indoor climate. In the single-slope solar greenhouses that are widely used in northern China, the thick wall on the north side of the greenhouse significantly affects heat storage performance during the winter. The greenhouse's heat budget cannot be calculated without knowing the temperature on both sides of the wall or without directly measuring the wall's heat flux. Although many of the mechanistic greenhouse models were designed using the traditional energy-balance-based modeling method, they generally performed well and were highly accurate (Sánchez-Molina et al., 2017; Rodriguez et al., 2015). However, the traditional modeling method usually requires multiple inputs such as the wall temperature, roof temperature and soil temperature, to simulate the resulting air temperature; this limits its applicability to real greenhouses where farmers need to predict the future greenhouse climate. In this paper, a new, simple model is introduced. Its simplicity derives from embedding a group of conservation equations relating to the boundary conditions. The steady-state equation series is solved in each transient simulation step to simplify the user's input conditions. To obtain the boundary conditions for each step, a feasible assumption is made to simulate the wall's future temperature distribution with the help of a weather forecast based on the finite difference method or finite volume method (Zhang et al., 2019b). However, for the greenhouse energy budget, only the temperature on both sides of the wall is needed, otherwise it would take up too much computational load. Therefore, a novel, easy-to-use wall temperature estimation method based on the energy balance was adopted for the environment model. It should be pointed out that few models have been developed to date that employ a mechanistic method combining temperature and humidity for use in Chinese solar greenhouses.

In this paper, several prior equations are integrated into the model to act as the mechanisms and middle links that exist in a real scenario. The final model was primarily chosen for its rigorous design and its similarity to the scenarios. Although some imperfections remain, it provides a method that serves as an example for the modelling. To summarize, the main contributions are as follows:

(i) A new greenhouse climate model is proposed that includes a novel and easy-to-use wall temperature estimation method based on the energy balance. With the help of the embedded group of conservation equations, the greenhouse boundary temperatures can be simulated rather than having to measure the boundary temperature at each time step. Therefore, the number of model inputs is reduced, and the model can estimate the future greenhouse climate using only the current or predicted weather variables.
(ii) Several typical management measurements were considered and then validated, such as: arbitrarily defining the vents' opening angle and the time they remain open, the time the greenhouse vents are completely closed, and whether to use the thermal insulation blanket as a roof covering. These aspects are not usually considered in climate models for Chinese solar greenhouses.
(iii) The model is computationally light and fast, and was calibrated and validated using data from different seasons and from different years.
(iv) The validation can be carried out in greenhouses of different sizes (and constructed from different materials) by switching the physical parameters; thus, the model is flexible and widely applicable. This was demonstrated by validating the proposed model in two greenhouses, each having a different size and located at different sites.
(v) The greenhouse temperature and humidity are simulated together using a mechanistic model – this is the first study to do so for Chinese solar greenhouses.

2. Materials and methods

This section summarizes the greenhouses where the experimental results were obtained for this work, the equipment used for the data

collection and the software tools employed for the model implementation.

2.1. Experiment description

2.1.1. Experimental greenhouse

The model validation was carried out using data from two different greenhouses. One is located in Xiaotangshan, at the National Precision Agriculture Demonstration Base (Greenhouse A, 40°18′ N, 116°47′ E), Changping District, Beijing, China, where the data from 2016 and 2019 were collected. The second greenhouse is located in Fangshan, on Hongke farm (Greenhouse B, 39°63′ N, 115°98′ E), Fangshan District, Beijing, where the data were gathered during 2019 and 2020 (Fig. 1).

Both greenhouses were the typical single-slope solar greenhouse-type with polyethylene (PE) film on the roof and a wall on the north side. The north wall of Greenhouse A is composed of bricks and gravelly soil whereas the north wall of Greenhouse B is made of hollow concrete blocks (Fig. 2). A cucumber crop was planted, and drip irrigation was installed, adopting a north–south cultivation line in Greenhouse A, and an east–west cultivation line in Greenhouse B. The 0.005 mm thick polyethylene film covers both greenhouses from the ground up to prevent soil evaporation. Greenhouse A is 50 m long, 7 m wide and 3.6 m high whereas Greenhouse B is 80 m long, 7.5 m wide and 4.2 m high.

2.1.2. Data collection

At each site, Davis Vantage Pro& Plus (Davis Instruments, Hayward, USA) outdoor weather stations were installed to measure the total solar radiation (range, 0–1800 W m^{-2}; accuracy, ±5%), wind speed (range, 0–67 m s^{-1}; accuracy, ±5%), air temperature (range, −40 - +65 ℃; accuracy, ±0.5℃), and relative humidity (range, 0–100%; accuracy, ±3%) (Fig. 3 (a)). Davis-6162 (Davis Instruments, Hayward, USA) weather stations were installed in the center of the greenhouses to measure the air temperature and relative humidity at a height of 1 m, solar radiation at a height of 1.5 m and soil temperature at a depth of 0.5 m (Fig. 3 (b)(c)). Considering the variables' rate of change, especially that for solar radiation, all the above data were measured and recorded at 15-minute intervals.

3. Model description

This section describes the proposed greenhouse climate model, where the new wall-temperature estimation method based on energy balance is introduced. Moreover, the opening and closing angles of the vents, and the thermal insulation blanket covering, are considered in the equations. The description of each model parameter and variable is given in the Appendix A nomenclature table. Furthermore, the tables in Appendix B summarize the values for the different model constants and variables.

3.1. Climate model

Under the assumption that air is transparent to solar radiation, the energy source terms for the air in the greenhouses belong to 5 sub-mechanisms: the ventilation energy source term, $q_v(t)$, W; the air leakage energy source term, $q_{lea}(t)$, W; the convective energy source term, $q_c(t)$, W; the water vapor liquidation energy source term, $q_{liq}(t)$, W; and the plant energy source term, $q_p(t)$, W (Fig. 4). The greenhouses' energy budget has a combined effect on the indoor temperature and humidity. The corresponding equation is given below:

$$\frac{dT(t)}{dt}*\rho*c_p*v + h(t)*\rho*c_{pw}*v*\frac{dT(t)}{dt} = q_v(t) + q_{lea}(t) + q_c(t) + q_{liq}(t) + q_p(t) \tag{1}$$

which can be simplified as,

$$\frac{dT(t)}{dt} = \frac{q_v(t) + q_{lea}(t) + q_c(t) + q_{liq}(t) + q_p(t)}{\rho*v*(c_p + c_{pw}*h(t))} \tag{2}$$

where, T is the indoor air temperature, K; h is the indoor absolute humidity, kg kg^{-1}; t is time, s; ρ is the air density, (1.293) kg m^{-3}; c_p is the specific heat capacity of the air, (1005) J kg^{-1} K^{-1}; c_{pw} is the specific heat capacity of the water vapor, (1850) J kg^{-1} K^{-1}; and v is the greenhouse volume, m^3.

The humidity equation was obtained by mass conservation. The greenhouses' humidity source terms come from the ventilation humidity source term, $s_v(t)$, kg kg^{-1} s^{-1}; the air leakage humidity source term, $s_{lea}(t)$, kg kg^{-1} s^{-1}; and the plant humidity source term, $s_p(t)$, kg kg^{-1} s^{-1}. The equation is given as follows,

$$\frac{dh(t)}{dt} = s_v(t) + s_{lea}(t) + s_p(t) \tag{3}$$

3.1.1. Ventilation source

This model includes the operations that affect the indoor climate, such as the vent opening angle and whether or not the thermal insulation cover is deployed. The natural ventilation adopted in this experiment relied on two rectangular vents at the top and bottom of the greenhouse. The opening angle, θ, is used to define the size of the vent opening. The driving force of the natural ventilation can be divided into thermal pressure ventilation and wind pressure ventilation (Roy et al., 2002), where the thermal pressure ventilation rate can be described in the following way:

In the case of both the upper and lower vents being open (Ma et al., 2008; NY/T 1451–2018, 2018),

$$L_T(t) = \mu_a(\theta_a(t))*A_{va}(t)*\sqrt{\frac{2*\left(\frac{T(t)}{T_o(t)} - 1\right)*g*H}{\left(\frac{T(t)}{T_o(t)}\right)^2*\left(\frac{\mu_a(\theta_a(t))*A_{va}(t)}{\mu_b(\theta_b(t))*A_{vb}(t)}\right)^2 + \frac{T(t)}{T_o(t)}}} \tag{4-1}$$

Fig. 1. Experimental greenhouses A (left) and B (right).

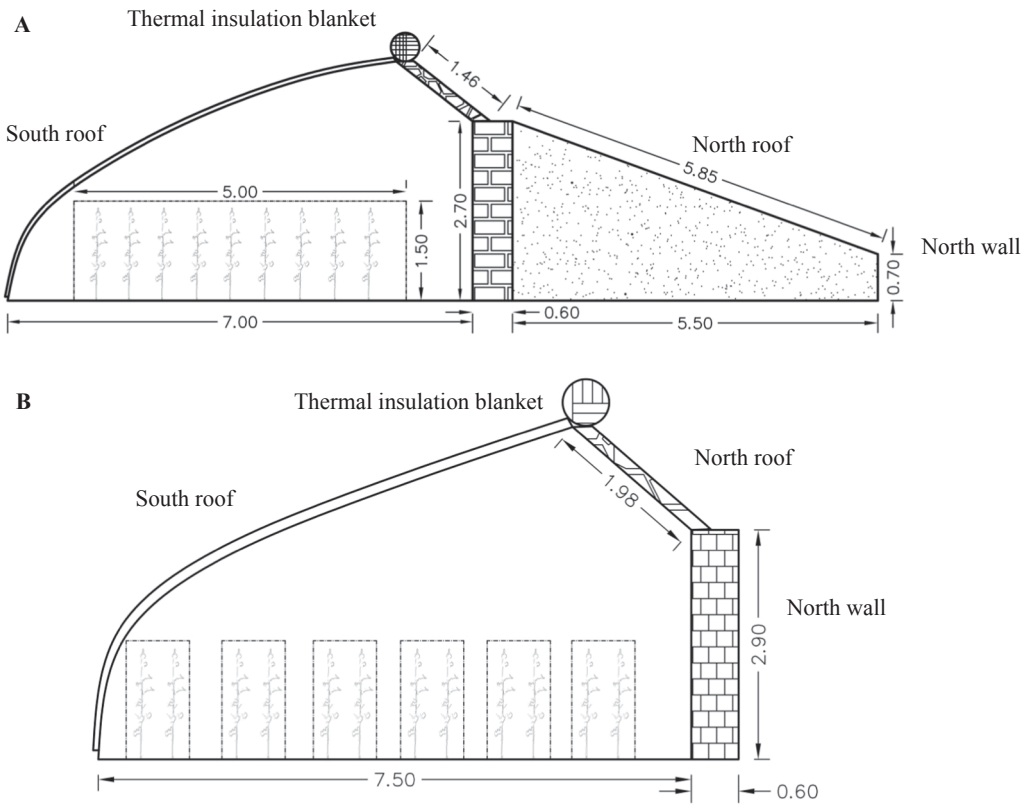

Fig. 2. Diagram of the structural dimensions (in meters) for greenhouses A and B.

Fig. 3. Sensors used for data collection.

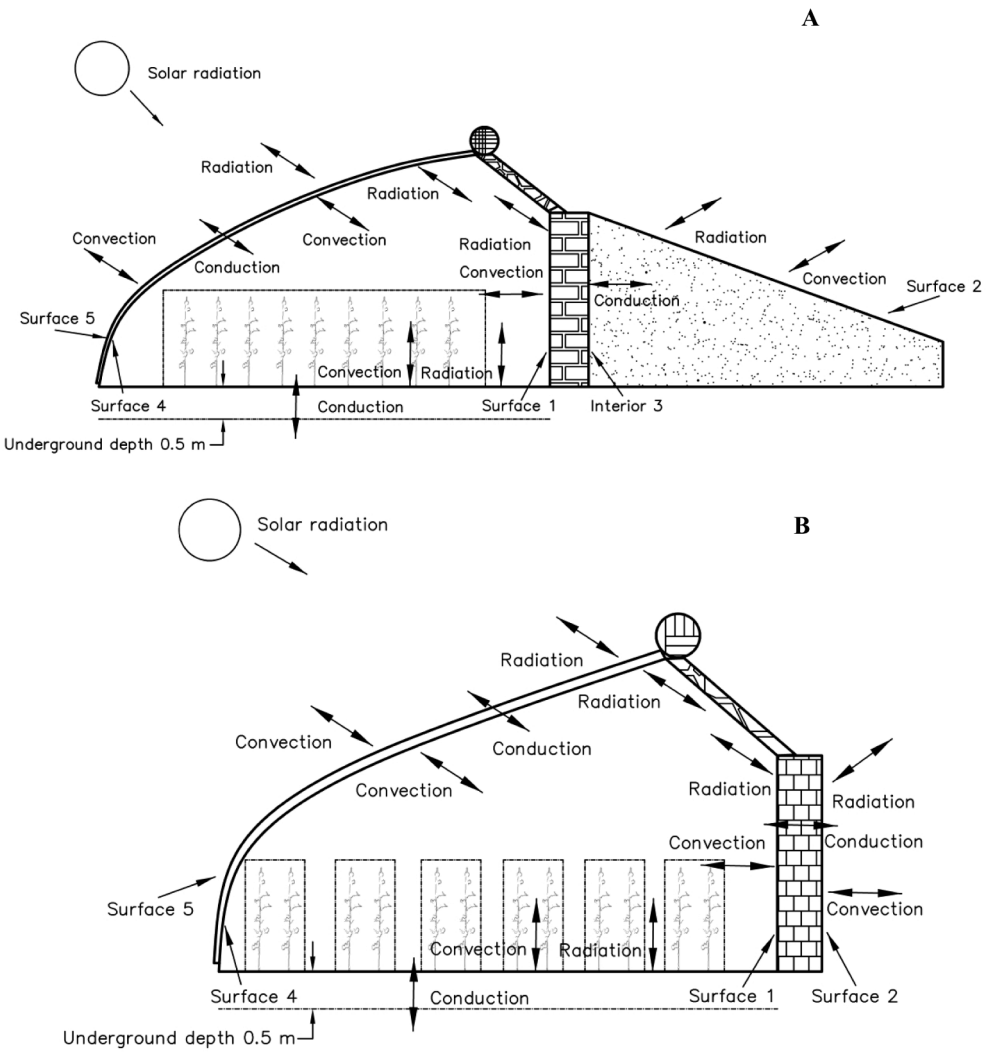

Fig. 4. Energy budget in greenhouses A and B.

$$A_{va}(t) = A_a * \left(sin \frac{\theta_a(t)}{2} \right) * 2 \tag{4-2}$$

$$A_{vb}(t) = A_b * \left(sin \frac{\theta_b(t)}{2} \right) * 2 \tag{4-3}$$

In the case of only the upper vent being open

$$L_T(t) = \mu_a(\theta_a(t)) * \frac{A_{va}(t)}{2} * \sqrt{\frac{\left(\frac{T(t)}{T_o(t)} - 1 \right) * g * H}{\left(\frac{T(t)}{T_o(t)} \right)^2 + \frac{T(t)}{T_o(t)}}} \tag{4-4}$$

where, L_T is the thermal pressure ventilation rate, $m^{-3}\ s^{-1}$; A_{va} is the open area of the upper vent, m^2; A_{vb} is the open area of the lower vent, m^2; A_a is the area of the upper vent plate (the movable part of the roof), m^2; A_b is the area of the lower vent plate, m^2; θ_a is the opening angle of the upper vent, °; θ_b is the opening angle of the lower vent, °; μ_a is the thermal pressure ventilation coefficient of the upper vent; μ_b is the thermal pressure ventilation coefficient of the lower vent ($\mu = 0.18$ when $\theta = 0$–15; $\mu = 0.33$ when $\theta = 15$–30; $\mu = 0.44$ when $\theta = 30$–45; $\mu = 0.53$ when $\theta = 45$–60; $\mu = 0.62$ when $\theta = 60$–90); If the greenhouse vents are opened (by rolling back the roof film), A_{va} and A_{vb} are input directly, with a corresponding μ of 0.62. g is the gravitational acceleration, 9.81 m s^{-2}; H is the height of the upper vent, m; and T_o is outdoor air temperature, K.

The wind pressure ventilation rate is expressed easily as an empirical equation (NY/T 1451–2018, 2018):

$$L_w(t) = \beta * A_{va}(t) * V_e(t) \tag{5}$$

where, L_w is the wind pressure ventilation rate, $m^{-3}\ s^{-1}$; β is the wind pressure coefficient (which is 0.5–0.6 when the wind direction is perpendicular to the vent and 0.25–0.35 when the wind direction is inclined), and V_e is the outdoor wind speed, m/s.

The ventilation energy source term, $q_v(t)$, is given by the following equation:

$$L(t) = \sqrt{L_T(t)^2 + L_w(t)^2} \tag{6}$$

$$q_v(t) = L(t) * \rho * c_p * (T_o(t) - T(t)) \tag{7}$$

$$s_v(t) = \frac{(h_o(t) - h(t)) * L(t)}{V} \tag{8}$$

where, L is the total ventilation rate, $m^{-3}\ s^{-1}$; and h_o is the outdoor absolute humidity, kg kg^{-1}.

3.1.2. Air leakage source

The air leakage rate has been studied for many years using the gas tracing method (Tong et al., 2008; Tong et al., 2009; Boulard et al.,

2017). In Chinese solar greenhouses, the air leakage rate varies widely from 0.13 to 2.31 h^{-1}, depending on the tightness of the cover, the wind speed, the solar radiation, and the temperature difference between the indoor and outdoor air (Tong et al., 2008; Tong et al., 2009; Zhang et al., 2019b). Using N_2O as the tracer gas, Boulard et al. (2017) found that the air leakage rate ranged from 0.075 to 0.09 h^{-1} at a wind speed of 0 ~ 0.9 m s^{-1} in a glass greenhouse. The empirical constant parameter seems to cause significant errors when applied to a real greenhouse, and even more so between new and old greenhouses. In this case, the following equation, which considers the tightness of the cover, the wind speed and the temperature difference, is the optimal estimation for the air leakage rate (Jolliet et al., 1991; Ahamed et al., 2018):

$$n_t = A_r * \eta_r * \sqrt{\beta^2 * V_e(t) + \eta_T^2 * (T(t) - T_o(t))} * \frac{3600}{V} \tag{9}$$

where, n_t is the air leakage rate, h^{-1}; A_r is the area of the transparent roof, m^2; η_T is the temperature difference factor (0.16, m s^{-1} $K^{-1/2}$); V_e is the wind speed, m s^{-1}; and η_r is the characterization of the tightness of the roof to air infiltration. Therefore, the air leakage energy source term, $q_{lea}(t)$, is described as follows:

$$q_{lea}(t) = \frac{n_t}{3600} * \rho * c_p * v * (T_o(t) - T(t)) \tag{10}$$

$$s_{lea}(t) = (h_o(t) - h(t)) * \frac{n_t}{3600} \tag{11}$$

3.1.3. Water vapor liquidation source

Water vapor liquidation is a phase-change mechanism that occurs when the air humidity is saturated; this has an impact on the greenhouse air temperature and humidity. The equations for these phenomena are described below (Snyder and Shaw, 1984):

$$P_s(T(t)) = 610.78 * e^{\left(\frac{T(t)-273.15}{T(t)-34.85} \times 17.2694\right)} \tag{12}$$

$$P_w(t) = \frac{h(t) * P}{0.622 + h(t)} \tag{13}$$

$$RH(t) = \frac{100 * P_w(t)}{610.78 * e^{\left(\frac{T(t)-273.15}{T(t)-34.85} * 17.2694\right)}} \tag{14}$$

$$h_s(T(t)) = 0.622 * \frac{P_s(T(t))}{P - P_s(T(t))} \tag{15}$$

where, $P_s(T(t))$ is the pressure of the saturated water vapor at T(t), pa; P is atmospheric pressure, pa; P_w is the water vapor pressure, pa; RH is the relative humidity, %; and $h_s(T(t))$ is the saturated humidity at T(t), kg kg^{-1}. So, when h(t) is higher than $h_s(T(t))$, the water vapor liquidation energy source term can be calculated in the following way:

$$q_{liq}(t) = \gamma * (h(t) - h_s(T(t))) * v * \rho \tag{16}$$

where, γ is the water evaporation constant, 2257600 J kg^{-1}. In this case, after liquidation, $h(t) = h_s(T(t))$ Alternately when h(t) is lower than $h_s(T(t))$:

$$q_{liq}(t) = 0 \tag{17}$$

3.1.4. Plant source

In general, the plant energy source term comes from the sensible heat exchange between the canopy and the surrounding environment, and from the heat released by condensation onto the canopy. The plant humidity source term derives from transpiration and condensation. In the above mechanisms, the canopy temperature is a necessary parameter. In this case, neglecting the sensitive heat exchange, the canopy temperature is assumed to be equal to the air temperature. Thus, the canopy's transpiration rate is described as follows (Boulard et al., 2017):

$$m_t(t) = \frac{LAD * \rho * C_p}{\zeta * \gamma} * \frac{P_s(T(t)) - P_w(t)}{r_a(t) + r_s(t)} \tag{18}$$

where, m_t is the transpiration rate, kg m^{-3} s^{-1}; LAD is the leaf area density, m^{-1}; r_a is the aerodynamic resistance, s m^{-1}; ζ is the psychrometric constant (value, 67.17 Pa K^{-1}); and r_s is stomatal resistance of the cucumber in relation to the irrigation conditions and the microclimate, s m^{-1}. r_a can be defined by the following formula (Boulard and Wang, 2002):

$$r_a(t) = 220 * \frac{l^{0.2}}{U^{0.8}} \tag{19}$$

where, l is the characteristic length (length of leaf), m; and U is the air speed in the crop zone, m s^{-1}. Solar radiation is the main meteorological factor affecting stomatal resistance in cucumber. The relationship between the solar radiation and the stomatal resistance in cucumber follows an exponential function, depending on the season of the year (Huang et al., 2020),

for the spring season, $r_s(t) = 144.3 + 1440.4 \cdot exp(-0.0124 * R_{sc}(t))$ (20)

$$r_s(t) = 224.4 + 1485.9 \cdot exp(-0.0185 * R_{sc}(t)) \tag{21}$$

$$R_{sc}(t) = (1 - exp(-K_c * LAI)) * R_s(t) * \tau \tag{22}$$

where, R_{sc} is the solar radiation absorbed by the crop canopy per second, W m^{-2}; R_s is the outdoor solar radiation intensity, W m^{-2}; τ is the short-wave transmissivity of the roof; K_c is the radiation attenuation coefficient, which was higher for the autumn cycle (0.86) than for the spring cycle (0.63) (Medrano et al., 2005); and LAI is the leaf area index.

The condensation rate on the canopy can be expressed using the following formula (Gerlein-Safdi et al., 2018):

$$m_c(t) = 0.622 * LAD * \rho * g_h(t) * \left(\frac{P_w(t) - P_s(T(t))}{p}\right) \tag{23}$$

where, m_c is the condensation rate on the canopy, kg m^{-3} s^{-1}, and g_h is the water vapor conductivity in the leaf boundary layer, m s^{-1}, which is a variable related to the Lewis number (N_{Le}) and the r_a,

$$g_h(t) = \left(r_a(t) * N_{Le}(t)^{2/3}\right)^{-1} \tag{24}$$

With

$$N_{Le}(t) = \frac{\alpha_a(t)}{D_w(t)} \tag{24-1}$$

$$\alpha_a(t) = T(t) * 1.32 \times 10^{-7} - 1.73 \times 10^{-5} \tag{24-2}$$

$$D_w(t) = T(t) * 1.49 \times 10^{-7} - 1.96 \times 10^{-5} \tag{24-3}$$

and where, N_{Le} is the Lewis number, dimensionless; α_a is the air thermal diffusivity, m^2 s^{-1}; and D_w is the water vapor diffusivity, m^2 s^{-1}.

Thus, the plant energy and humidity source terms, $q_p(t)$, $s_p(t)$, are expressed as follows:

$$q_p(t) = m_c(t) * \gamma * v_p * \tau \tag{25}$$

$$s_p(t) = \frac{(m_t(t) - m_c(t)) * v_p}{\rho * v} \tag{26}$$

where, v_p is plant canopy volume, m^3.

3.1.5. Convective source

This section describes the new method proposed for estimating the wall temperature. The convective energy source terms come from the walls (f_w, W), the roof (f_r, W) and the ground (f_g, W). Thus, the convective energy source, $q_c(t)$, can be expressed as,

$$q_c(t) = f_w(t) + f_r(t) + f_g(t) \tag{27}$$

It is assumed that convective heat transfer is the only direct energy exchange mechanism between the internal surfaces and the indoor air, whereas heat conduction only affects the temperature of the internal surfaces, thus affecting the indoor air temperature indirectly. Therefore:

$$f_w(t) = A_{s1}{*}c_{wi}(t){*}(T_1(t) - T(t)) \tag{28}$$

$$f_r(t) = A_r{*}c_{ri}(t){*}(T_4(t) - T(t)) \tag{29}$$

$$f_g(t) = A_g{*}c_g(t){*}\left(T_g(t) - T(t)\right) \tag{30}$$

where, A_{s1}, A_r, and A_g are the areas of the wall, roof and ground, m^2, respectively; c_{wi}, c_{ri} and c_g are the convective transfer coefficients on the internal surfaces of the opaque wall, the transparent roof and the ground, W m^{-2} K^{-1}, respectively; T_g is the ground temperature, K; and T_1 and T_4 are the wall surface temperatures, which are estimated as described below.

The wall temperature calculation is performed using the following energy balance through the easy wall temperature estimating (EWTE) method. For the wall composed of two different materials (Greenhouse A), the wall energy balance is calculated by dividing the wall into three surfaces – the internal wall surface (S.1), the external wall surface (S.2), and the interior space between the different wall materials (I.3) (Fig. 4 (A)). For Greenhouse B, the equations are calculated without I.3 (Fig. 4 (B)).

The surfaces on both sides of the transparent roof are calculated - the internal roof surface (S.4) and the external roof surface (S.5). The equations are shown below, and are divided into two cases: with and without the cover configuration of the thermal insulation blanket.

Cover configuration without the thermal insulation blanket (on the wall surfaces)

For S.1, the energy balance belongs to the convective term, the conduction term, and the long-wave and solar radiation term:

$$\begin{aligned} &A_{s1}{*}c_{wi}(t){*}(T(t) - T_1(t)) + \frac{(T_3(t) - T_1(t)){*}Cd_{w1}}{Th_{w1}}{*}A_{s1} + \sigma{*}e_{wr}{*}\left(T_4(t)^4\right. \\ &\left. - T_1(t)^4\right){*}A_{s1}{*}x_{wr} + \sigma{*}e_{ws}{*}\tau_l{*}\left(T_o(t)^4 - T_1(t)^4\right){*}A_{s1}{*}x_{wr} \\ &+ \tau{*}R_s(t){*}A_r{*}x_{rw}{*}a_{s1} = 0 \end{aligned} \tag{31-1}$$

For S.2, the equation terms are similar to Eq. (31 1), with the addition of the solar radiation term:

$$\begin{aligned} &A_{s2}{*}c_{wo}(t){*}(T_o(t) - T_2(t)) + \frac{(T_3(t) - T_2(t)){*}Cd_{w2}}{Th_{w2}}{*}A_{s3} \\ &+ \sigma{*}e_{ws}{*}\left(T_o(t)^4 - T_2(t)^4\right){*}A_{s2} = 0 \end{aligned} \tag{31-2}$$

For I.3:

$$\frac{(T_1(t) - T_3(t)){*}Cd_{w1}}{Th_{w1}}{*}A_{s1} + \frac{(T_2(t) - T_3(t)){*}Cd_{w2}}{Th_{w2}}{*}A_{s3} = 0 \tag{31-3}$$

(on the roof surfaces)

In the same way, for S.4:

$$\begin{aligned} &A_r{*}c_{ri}(t){*}(T(t) - T_4(t)) + \frac{(T_5(t) - T_4(t)){*}Cd_r}{Th_r}{*}A_r + \sigma{*}e_{rw}{*}\left(T_1(t)^4\right. \\ &\left. - T_4(t)^4\right){*}A_r{*}x_{rw} = 0 \end{aligned} \tag{31-4}$$

and for S.5:

$$\begin{aligned} &A_r{*}c_{ro}(t){*}(T_o(t) - T_5(t)) + \frac{(T_4(t) - T_5(t)){*}Cd_r}{Th_r}{*}A_r + \sigma{*}e_{rs}{*}\left(T_o(t)^4\right. \\ &\left. - T_5(t)^4\right){*}A_r = 0 \end{aligned} \tag{31-5}$$

T_1, T_2, T_3, T_4 and T_5, are the temperatures of S.1, S.2, I.3, S.4 and S.5 (in K), respectively; A_{s1}, A_{s2}, A_{s3} and A_r are the areas of S.1, S.2, I.3 and the south roof (in m^2), respectively; Cd_{w1} is the thermal conductivity of the wall material close to S.1,W m^{-1} K^{-1}; Th_{w1} is the wall thickness between S.1 and I.3, m; Cd_{w2} is the thermal conductivity of the wall material close to S.2, W m^{-1} K^{-1}; Th_{w2} is the wall thickness between S.2 and I.3, m; σ is the Boltzmann constant, (0.0000000567) W m^{-2} K^{-4}; e_{ws}, e_{wr}, e_{rw} and e_{rs} are the long-wave radiation exchange coefficients from the wall to the sky, from the wall to the south roof, from the south roof to the wall and from the south roof to the sky, respectively; x_{wr} is the view factor from the wall to the south roof; x_{rw} is the view factor from the south roof to the wall; τ is the short-wave transmissivity of the south roof; τ_l is the long-wave transmissivity of the south roof; a_{s1} is the absorbed solar radiation coefficient of surface 1; and c_{wo} and c_{ro} are the convective transfer coefficients of the external wall and roof surfaces, W m^{-2} K^{-1}. The thermal conductivities of the greenhouse materials are shown in Table 1.

Please see Appendix C for the simulation of the cover configuration using the thermal insulation blanket.

Under the assumption of a diffuse-grey surface, the view factor is used to calculate the radiative heat transfer between the surfaces that are separated by transparent media (Modest, 1993). The view factor between the south roof and the north wall depends on the spatial relationship and the shielding medium, i.e., the plant canopy between them. The crop canopy height is 0.5 m in early April and early September, and 1.5 m in May, October, and November. With the aid of auxiliary surfaces, the view factor can be calculated between two objects that have a complex spatial relationship. The corresponding view factor calculation is shown in Fig. 5 and the equations are shown below. It should be noted that the equations in each case are the same (Eq. (31 6)), but the sizes of the parameters are different.

$$\begin{cases} x_{rw} = \dfrac{A_1 + A_2 - A_3}{2A_1}{*}\dfrac{A_2 + A_5 - A_4}{2A_2}{*}\dfrac{A_5 + A_7 - A_6}{2A_5} \\ x_{wr} = \dfrac{A_1{*}X_{rw}}{A_7} \end{cases} \tag{31-6}$$

Convective transfer is the main form of energy gain (or loss) from (or to) the indoor air; this has been studied for many years (Roy et al., 2002). When using different convective transfer models, deviations of up to ± 30% are seen in the annual cooling energy demand (Mirsadeghi et al., 2013). It is important to choose an appropriate convection model according to the specific building and the parameters available. Regarding Chinese solar greenhouses, at least 4 different models are necessary for the convective transfer coefficients.

Convective transfer coefficients on the external and internal surface of the opaque wall

The Building Loads Analysis and System Thermodynamics (BLAST) model is comprehensive as it considers both the forced ($c_{wo,\ for}$, W m^{-2} K^{-1}) and the natural ($c_{wo,\ nat}$, W m^{-2} K^{-1}) convection components on the external wall surface (Walton, 1981; McClellan and Pedersen, 1997):

$$c_{wo}(t) = c_{wo,for}(t) + c_{wo,nat}(t) \tag{31-7}$$

$c_{wo,\ for}$ is estimated using the following equation, which is based on wind tunnel experiments using rectangular plates (Sparrow et al., 1979):

$$c_{wo,for}(t) = 2.537{*}W_f{*}R_f{*}\left(\frac{Pe{*}V_f(t)}{A}\right)^{1/2} \tag{31-8}$$

where, W_f is the wind direction modifier, with 1 for the windward surface and 0.5 for the leeward surface; Pe is the surface perimeter, m; A is the surface area, m^2; R_f is the surface roughness multiplier, 1.67 for brick and 1.52 for concrete (Walton, 1981); and V_f is the free-stream wind speed, m s^{-1}. In this case, the free-stream wind speed is

Table 1
Thermal conductivity of the materials (Zhang et al., 2019b; Carlini et al., 2020; Ahamed et al., 2018).

	Clay Brick	Gravelly soil	Polyethylene	Hollow block	Soil
Thermal conductivity(W m^{-1} K^{-1})	0.81	1.80	0.38	1.02	1.4

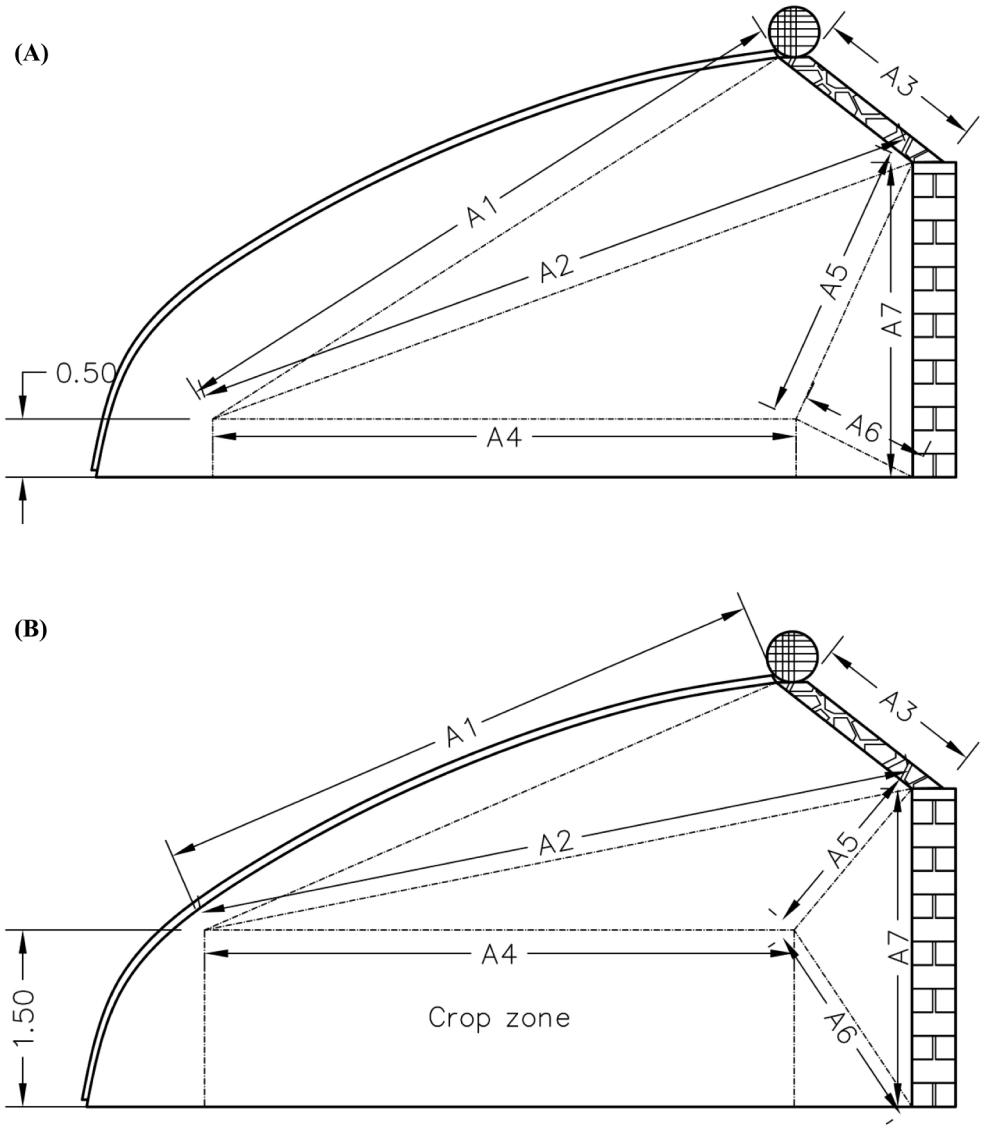

Fig. 5. Calculation of the view factor when the crop height is 0.5 m (A) and 1.5 m (B).

estimated using the wind profile model and the wind speed measured 2.5 m above the ground (Boulard et al., 2010). $c_{wo,\ nat}$ is the natural component of convection, which is calculated using the following equations (Walton, 1983; Mirsadeghi et al., 2013):

$$c_{wo,nat}(t) = 9.482*\frac{(|T_2(t) - T_o(t)|)^{\frac{1}{3}}}{7.238 - |cos\varphi|}, (T_2 > T_o) \quad (31\text{-}9)$$

$$c_{wo,nat}(t) = 1.810*\frac{(|T_2(t) - T_o(t)|)^{\frac{1}{3}}}{1.382 + |cos\varphi|}, (T_2 < T_o) \quad (31\text{-}10)$$

where, φ is the surface plane angle in relation to the ground plane, °.

The convective coefficient on the internal wall surface is estimated considering only the natural component:

$$c_{wi}(t) = 9.482*\frac{(|T_1(t) - T(t)|)^{\frac{1}{3}}}{7.238 - |cos\varphi|}, (T_1 > T) \quad (31\text{-}11)$$

$$c_{wi}(t) = 1.810*\frac{(|T_1(t) - T(t)|)^{\frac{1}{3}}}{1.382 + |cos\varphi|}, (T_1 > T) \quad (31\text{-}12)$$

Convective transfer coefficients on the external and internal surfaces of the transparent roof

A variety of roof convection models have been applied to different types of greenhouses, usually a wind speed-dependent model for the exterior and a temperature-difference model for the interior (Roy et al., 2002). In this case, the following equations were adopted to estimate the external and internal convection transfer coefficients, applied to conditions where there is a polyethylene-covered greenhouse, above which the wind speed is measured (5.6 m above the ground) at less than 6.3 m s^{-1} (Papadakis et al., 1992):

$$c_{ro}(t) = 0.95 + 6.76*Ve(t)^{0.49} \quad (31\text{-}13)$$

$$c_{ri}(t) = 2.21*(T(t) - T_4(t))^{\frac{1}{3}}, (0.3 < T - T_4 \leq 13.8^{\circ}C) \quad (31\text{-}14)$$

The long-wave radiation exchange coefficient between two grey-body surfaces can be described as follows (Liu and Zhang, 2011):

$$e_{ij} = \left(e_i^{-1} + e_j^{-2} - 1\right)^{-1} \quad (31\text{-}15)$$

where, e_{ij} is the long-wave radiation exchange coefficient, and e_i and e_j are the long-wave emissivity of two radiation objects, which are shown in Table 2.

The sky emissivity variable (e_s) is related to the outdoor air temperature (T_o, K) and the outdoor water vapor pressure (P_{wo}, Pa) (Kustas et al., 1994):

$$e_s(t) = 0.642(P_{wo}(t)/T_o(t))^{1/7} \quad (31\text{-}16)$$

The wall temperature is simulated using several outdoor climate variables, which can be provided by the weather forecast. In contrast to the wall temperature simulation, the ground temperature simulation requires the boundary temperature at a set depth beneath the ground. The ground temperature is simulated after taking the initial soil temperature at a depth of 0.5 m; this is measured using a temperature probe:

For the ground surface:

$$A_g{*}c_g(t){*}\big(T(t) - T_g(t)\big) + \frac{\big(T_d(t) - T_g(t)\big){*}Cd_g}{Th_g}{*}A_g + \sigma{*}e_{gr}{*}\big(T_4(t)^4 - T_g(t)^4\big){*}A_g{*}x_{gr} + \sigma{*}e_{gs}{*}\tau_l{*}\big(T_o(t)^4 - T_g(t)^4\big){*}A_g{*}x_{gr} + (R_s(t){*}\tau{*}x_{gr}{*}A_g - R_{sc}(t){*}A_p){*}a_g = 0 \quad (32\text{-}1)$$

For a depth of 0.5 m beneath the ground:

$$\frac{dT_d(t)}{dt}{*}\rho_g{*}c_{pg}{*}v_g = \frac{\big(T_g(t) - T_d(t)\big){*}Cd_g}{Th_g}{*}A_g \quad (32\text{-}2)$$

where, T_g is the ground surface temperature, K; T_d is the below-ground temperature at a depth of 0.5 m, K; ρ_g is the soil density, (1975) kg m^{-3}; c_{pg} is the specific heat capacity of the soil, (1480) J kg^{-1} K^{-1}; v_g is the soil volume, m^3; e_{gr} and e_{gs} are the long-wave radiation exchange coefficients from the ground to the roof and sky; x_{gr} is the view factor from the ground to the roof; A_g is the ground surface area, m^2; A_p is the plant area, m^2; a_g is the absorbed solar radiation coefficient of the ground (0.92); c_g is the convective transfer coefficient of the ground, W m^{-2} K^{-1}; Th_g is the thickness of the ground, 0.5 m; and Cd_g is the thermal conductivity of the soil, W m^{-1} K^{-1}. The convective transfer coefficient of the ground is estimated using the following equation, which was developed in a large-scale greenhouse (De Halleux, 1989),

$$c_g = 1.86{*}(|T_g(t) - T(t)|)^{\frac{1}{3}} \quad (32\text{-}3)$$

3.2. Model implementation and validation

The model system was implemented using Matlab and Simulink. The Root Mean Squared Error (RMSE) and Mean Error (ME) were used to evaluate the errors between the calculated and the measured data, as expressed in Eqs. (33,34):

$$RMSE = \sqrt{\frac{\sum_{i=1}^{N}(C_{ai} - M_{ei})^2}{N-1}} \quad (33)$$

$$ME = \frac{|C_{ai} - M_{ei}|}{N} \quad (34)$$

where, C_{ai} is the estimated value, M_{ei} is the measured value, and N is the sample size.

4. Results and discussion

This section presents the validation results for the proposed model. The temperature and humidity results are also given. The model was validated during different seasons with data from Greenhouse A and Greenhouse B. Note that the accuracy of the model is demonstrated not only by validating the model in different seasons and in different years, but also by calibrating it in one greenhouse and validating it in the other. The calibration process was performed in MATLAB implementing the Monte Carlo method to estimate the global model parameters, resulting in the table showing the calibrated model parameters in Appendix B.

4.1. Model performance on a single day

In this section, the thermal and mass (humidity) performance is validated on a single day when the vents are closed. Several middle links in this model are analyzed to show the energy and mass budget of the greenhouse. Subsequently, the ventilation is analyzed by simulating the greenhouse climate when the vents are open.

Fig. 6 shows the simulation and measurement when the vents are closed in Greenhouse A. The crop height is 1.5 m and the LAI is 2.55. The RMSE of the temperature is 2.6 K. The RMSE of the absolute humidity and the relative humidity are 3.1 g kg^{-1} and 14.6%, respectively. The simulation under closed-vent conditions is of great significance as it illustrates the model's performance. The curve fluctuation and peak value of the absolute humidity are consistent with the real situation, although the relative humidity error is striking due to the temperature difference. Fig. 7 shows that the thermal performance is also good when applied to Greenhouse B, with the temperature RMSE at 3.3 K. The RMSE of the absolute humidity and the relative humidity are 3.0 g kg^{-1} and 17.8%, respectively.

Compared to the dynamic models from other studies validated on typical days, the RMSE of T was 5.3 K with T increasing from 308 K to 343 K (Mohammadi et al., 2018). In Singh et al. (2006), the RMSE of T was 5.69 K with T increasing from 287 K to 301 K, and the RMSE of RH was 4.37% with the error ranging from 3.08% to 27.78% Notice that the error in the latter study was obtained with a temperature increase over 30 K, which demonstrates that the model is accurate in terms of the energy budget. This model also provides a leaf wetness risk that is based on simulating the crop canopy condensation (Fig. 6) which, when combined with temperature, can be a useful tool for a plant disease warning system (Zhao et al., 2011).

The indoor solar radiation intensity measured was higher at noon and lower at other times compared to the simulation (Fig. 8). A more precise method would be to adopt a variety of times to simulate τ. The transmittance is highest when the solar incidence angle is perpendicular to the roof, and gradually reduces as the angle increases (Soriano et al., 2004). However, the transmittance only changes slightly in the 0 to 60-degree incidence range, and decreases rapidly when the incident angle exceeds 60° (Zhang et al., 2020a). Thus, the roof transmittance value remains almost at the maximum during most of the daytime. Given the computational load needed to simulate it, and the consistency shown between the simulated and measured indoor solar radiation (Fig. 8), relying on the transmittance constant is feasible.

The air leakage rate varies from 0.2 h^{-1} to 0.6 h^{-1} and reaches its peak at noon. In a very tightly covered solar greenhouse with a span of 6.6 m and a ridge height of 3 m, the mean air leakage rate was 0.35 h^{-1} in the daytime and 0.15 h^{-1} at night (Tong et al., 2007). In another Chinese solar greenhouse, the air leakage rate measured using the carbon dioxide tracing method varied between 0.33 h^{-1} and 0.41 h^{-1} (Tong et al., 2007). Considering that the air leakage rate variable is positively related to wind speed, solar radiation, and the indoor/ outdoor temperature difference, the equation adopted in this model was able to simulate the air leakage rate accurately and proportionally.

The convective heat transfer coefficients used in this model have been proven to be applicable to other scenarios (De Halleux, 1989; Papadakis et al., 1992; Walton, 1983; Mirsadeghi et al., 2013). Of these,

Table 2
Long-wave emissivity of the objects and the long-wave radiation exchange coefficient estimated using Eq. (31–15).

Emissivity of objects	Wall (e_w)		Roof (e_r)		Thermal insulation blanket (e_b)	Sky (e_s)
Value	0.9		0.5		0.9	Eq. 31–16
Long-wave radiation exchange coefficient	e_{wr}	e_{rw}	e_{wb}	e_{bw}	e_{ws}	e_{rs}
Value	0.24	0.45	0.74	0.74	$(e_w{}^{-1} + e_s{}^{-2} - 1)^{-1}$	$(e_r{}^{-1} + e_s{}^{-2} - 1)^{-1}$

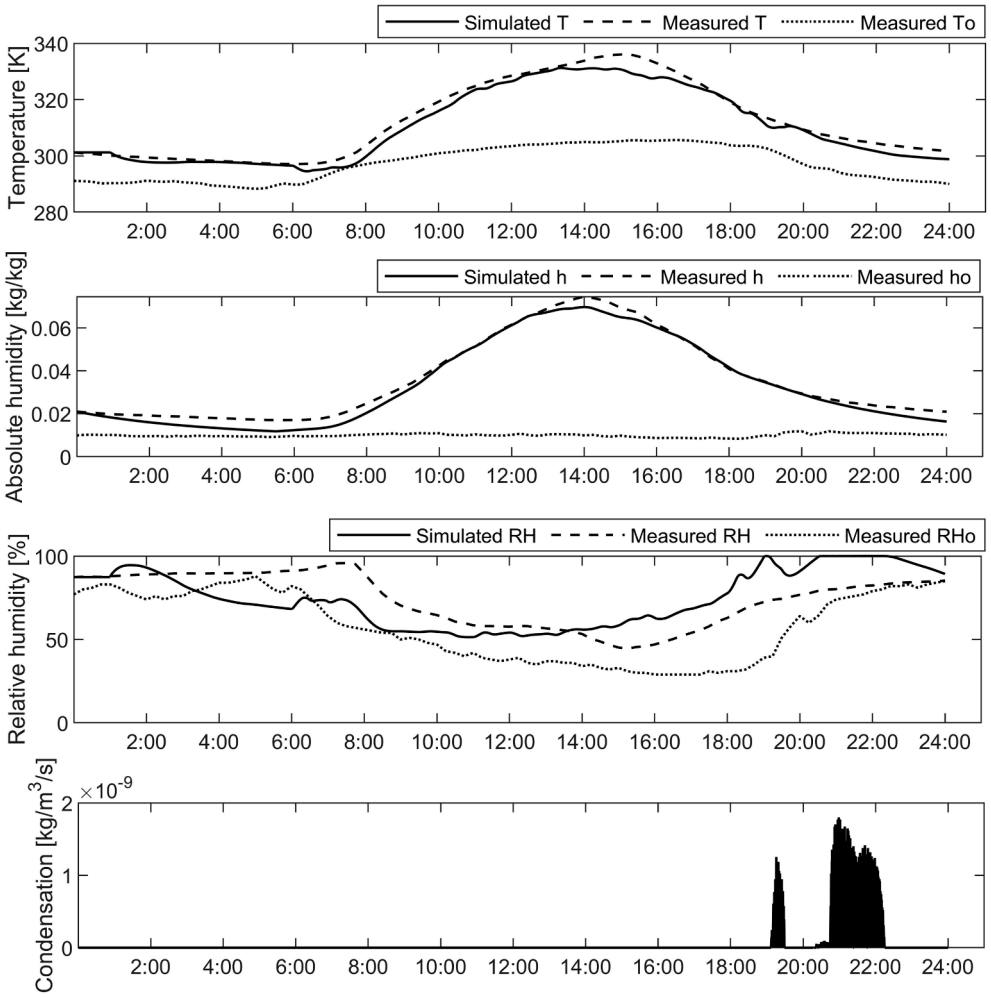

Fig. 6. Data set for the temperature, humidity, and crop canopy condensation under closed-vent conditions, recorded on 17 August 2019 in Greenhouse A.

the external roof coefficient was the highest while the internal wall coefficient was the lowest (Fig. 8). All the parameters peaked at noon, whereas the external wall, internal wall and external roof coefficients were close to 0 over night when the wind speed was low.

Transpiration in cucumber varies from 0 to 150 W m^{-2} in autumn with the LAI ranging from 2 to 3.5; this was measured using a sap-flow sensor in a Venlo greenhouse (Huang et al., 2020). The transpiration rate in Fig. 8 began to rise after 6:00 a.m. and reached its peak at noon; then, the transpiration rate gradually dropped to 0 after 18:00. This was similar to the transpiration rate measured by Huang et al. (2020) from 2 − 16 October 2018. Evapotranspiration is the main humidity source under closed-film conditions. Accurate transpiration rate simulation is an important middle link in humidity modeling.

Fig. 9 shows how the temperature increases and decreases in the energy budget. Based on the model assumption, the air is transparent to the solar radiation and is heated by convective heat transfer from the wall and soil surfaces; these absorb the solar radiation in the daytime, 34% of which is absorbed by the wall and 66% by the ground. Not all the solar radiation absorbed by the wall will be converted into air heating, and thus the process is simulated by solving the embedded conservative equation group for each second. The transparent roof is the main medium of greenhouse energy loss, accounting for 86% of losses in the daytime and 65% at night, followed by air leakage, which accounts for 14% of losses in the daytime and 23% at night. The ground is the main medium providing energy at night, but it is insufficient to offset the loss, and the net energy overnight is −19.5 MJ.

Fig. 10 shows the model's ventilation performance for different vent opening areas, in which the temperature curve and the absolute humidity curve indicate the energy and mass responses to the ventilation, respectively. The agreement between the measured and the simulated curves demonstrates the accuracy of the simulated ventilation rate. The RMSE of the temperature, absolute humidity, and relative humidity is 2.5 K, 1.1 g kg^{-1} and 8.6%, respectively. Fig. 10 also shows a significant positive correlation between the wind speed and the ventilation rate. The ventilation times are obtained from the hourly cumulative ventilation rate divided by the greenhouse volume - these are 2.23 h^{-1} when the opening area is 5 m^2 and 13.36 h^{-1} when the opening area is 10 m^2. Notice that this value is for the single-vent opening configuration, and would be higher if both the lower and upper vents were open.

4.2. Model performance on consecutive days

In this section, the model was validated on consecutive days in different seasons during 2016 and 2019. The number of consecutive days in each test amounted to 1 week, and the total days simulated amounted to four weeks. The outdoor weather station data was used as the model input and the validation data were taken from the indoor sensors. Different ventilation configurations were applied during the experiment along with the use of the thermal insulation blanket. The ME (Mean Error) and RMSE between the simulated and measured data are shown in Table 3.

4.2.1. Temperature performance

Figs. 11-14 show the input data set, which includes the outdoor

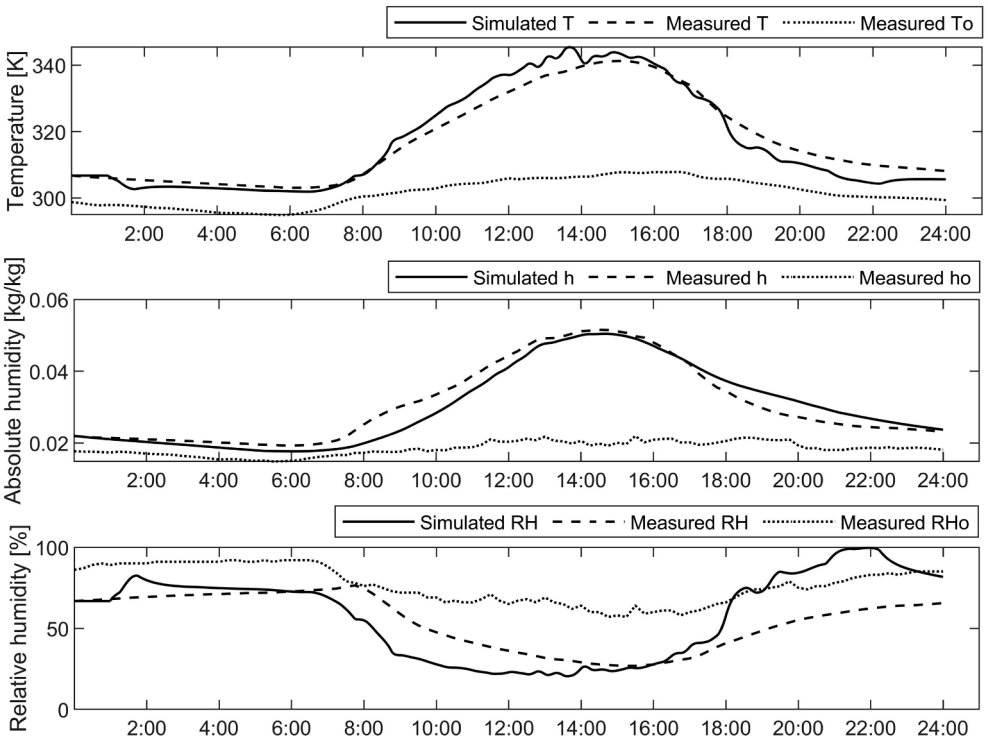

Fig. 7. Data set for the temperature and humidity under closed-vent conditions, recorded on 11 August 2020 in Greenhouse B.

temperature, outdoor humidity, outdoor solar radiation, wind speed, and the output. The simulated temperature fitted the real data measured in the spring, autumn and cold season (tests 1–4), with the ME and RMSE from 1.5 to 2.4 K, and from 2.0 to 2.9 K, respectively (Table 3). The temperature was underestimated in Fig. 14, which resulted in the RH exceeding the maximum saturation value. A similar phenomenon appeared in the semi-Quonset-type greenhouse simulation when the vents were closed in the cold season; here, the predicted RH value was higher than the measured value and the predicted T was lower than the measured value (Singh et al., 2006). Nonetheless, in Fig. 14, the model performed well under continuous low-temperature and low-illumination weather conditions from day 3 to day 6. The simulated temperature changed simultaneously and precisely in line with the solar radiation intensity, even under extremely low intensities (Figs. 11-14); this means that the model's simulated air temperature is sensitive to, and responds accurately to, changes in the outdoor solar radiation.

It should be pointed out that the validations were conducted in the same periods of the year for both Greenhouse A and Greenhouse B (Figs. 11-14), the data for which were not considered during the calibration process. As demonstrated by the figures and by the quantitative results in Table 3, the model provides very promising results when used in similar types of greenhouse (although of different sizes) as the one used for calibration purposes. It is worth remarking that this is the typical greenhouse structure found in China, and thus the model could be used to estimate the temperature and humidity of any of these greenhouses, simply by updating the greenhouse's structural parameters.

4.2.2. Humidity performance

The humidity performance values were good for weeks 1–4 with the ME and RMSE ranging from 6.9% to 13.1% and 8.8% to 16.6%, respectively, in the different seasons and the different greenhouses (Table 3). The simulation and measurement curves are perfectly consistent for the temperature, absolute humidity, and relative humidity (Figs. 11-14). The RH is sensitive to temperature, with the average variation in RH spatial distribution for a single-span greenhouse (with a floor area of 8 m × 20 m) being 13%, and where the maximum difference could be over 40% (Ahmed et al., 2019). Few mechanistic models for greenhouse humidity have been developed, with the exception of some CFD models (Boulard et al., 2017); this is due to the complexity of comprehensively considering the water vapor sources, which are estimated using a mass exchange model between the indoor and outdoor environments, as well as the liquidation model, condensation and leaf transpiration model. During the simulation, this study tried to consider all the middle links as far as possible, and the results are striking.

4.3. Schematic representation of the model: Inputs and outputs

This section describes how the model works with only 4 inputs and 3 initial-condition values. The model runs on the inputs shown in Fig. 15, which can be provided by the weather station or from weather forecast data. All the middle links are simulated by adopting proper equations developed under similar conditions in the first and second layers. In addition, prior to the simulation, the size of the construction and the properties of its physical materials should be given. Only 3 initial values were defined at the outset; these were the initial temperature T, the initial humidity h, and the initial soil T_d. The results show that the model is accurate for at least 7 days without recalibrating the initial conditions. Reducing the required number of sensor inputs not only lowers the cost, but also avoids any inconvenience caused by faulty sensors. Compared to the current models, it has been shown that the wall temperature or wall flux are necessary inputs (Li et al., 2020; Sánchez-Molina et al., 2017). Many models require sensors to be placed on the ground, the wall, and in the roof. When applied in practice, any sensor fault will lead to the model failing to run. The model in this paper not only effectively reduced the amount of inputs, but it could also be transplanted successfully to another greenhouse without affecting the model's performance from season to season or from year to year.

5. Conclusions

The model described in this paper allows one to estimate the

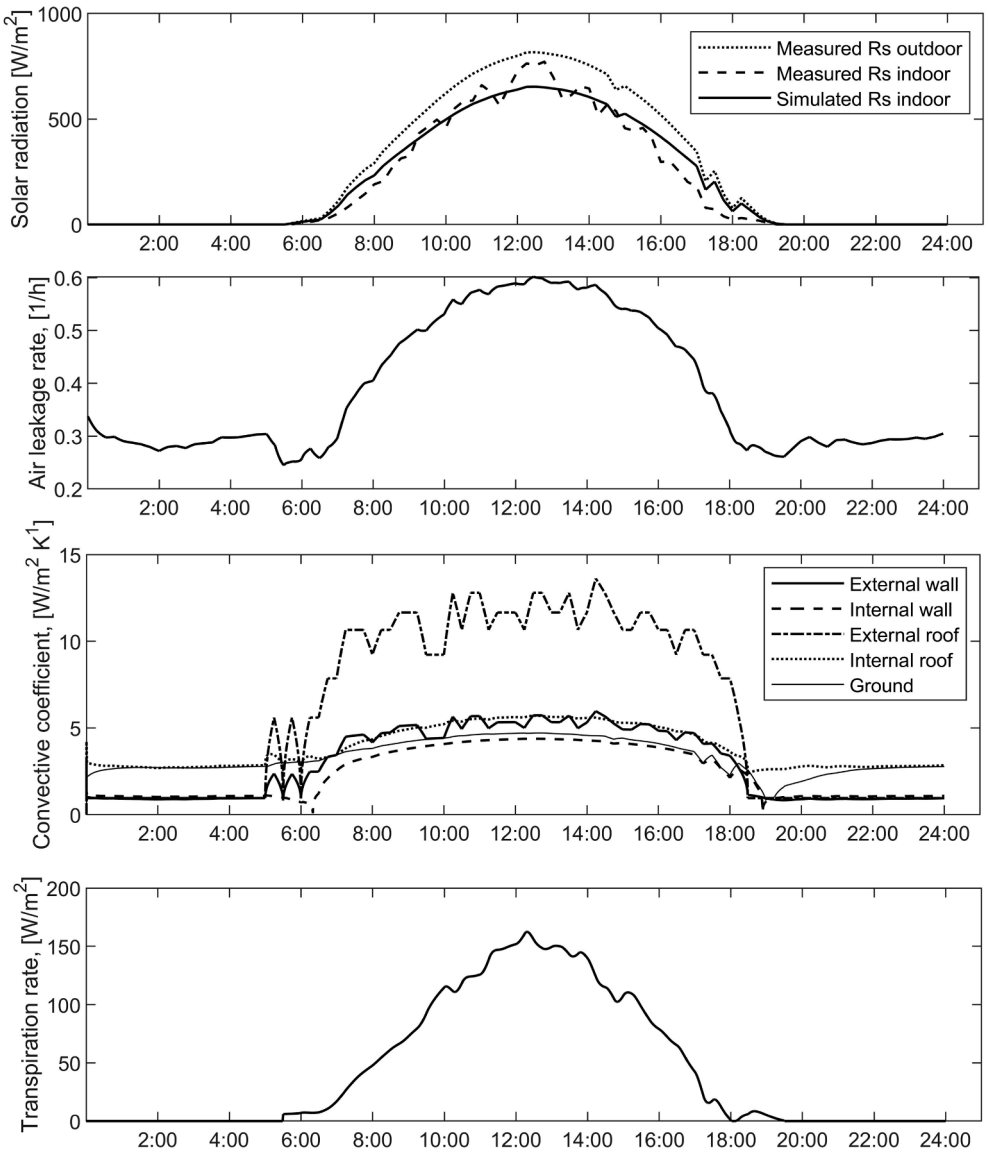

Fig. 8. Data set for the simulated solar radiation, air leakage rate, convective transfer coefficient and crop transpiration rate on 17 August 2019 in Greenhouse A.

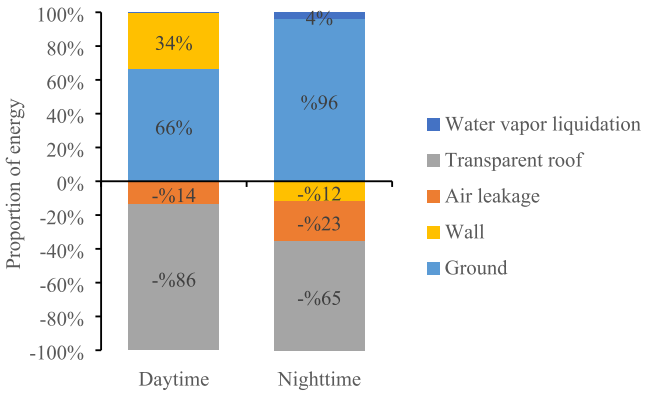

Fig. 9. The proportion of gain and loss to the greenhouse's energy for each link under closed-vent conditions on 17 August 2019 in Greenhouse A.

temperature and humidity of a typical Chinese solar greenhouse using only the solar radiation, outdoor temperature, outdoor humidity, and wind direction and speed, as the model inputs. The model also includes a variety of management modes, such as the vent opening angle, the time the vents are open or closed, and the time that the thermal insulation blanket covers the roof. The RMSEs for the predicted temperature on three separate days were 2.6 K, 3.3 K, 2.5 K, respectively, while the RMSEs for the predicted relative humidity were 14.6%, 17.8% and 8.6%, respectively. The RMSEs for the predicted temperature on four consecutive days (1 week for each test) remained in the 2.0 K to 2.8 K range while the RMSEs for the predicted relative humidity remained in the 8.8% to 16.6% range during different seasons in 2016 and 2019. Therefore, the simple model proposed has demonstrated its promising accuracy and ability to predict the future environmental behavior inside a greenhouse.

In addition, the model was validated in a second greenhouse, which was a different size to the one used for the calibration. Notice that only the physical model parameters were modified, such as the greenhouse volume, the roof and wall areas, the wall materials and so on; this is because the other parameters are common to both greenhouses. The validation for the transplanted modeling was good, which means that this model (or its methodology) can be widely adapted to typical Chinese solar greenhouse of different sizes.

In terms of ensuring the resolution and accuracy, the proposed model has the advantage of being fast. The most time-consuming part of the

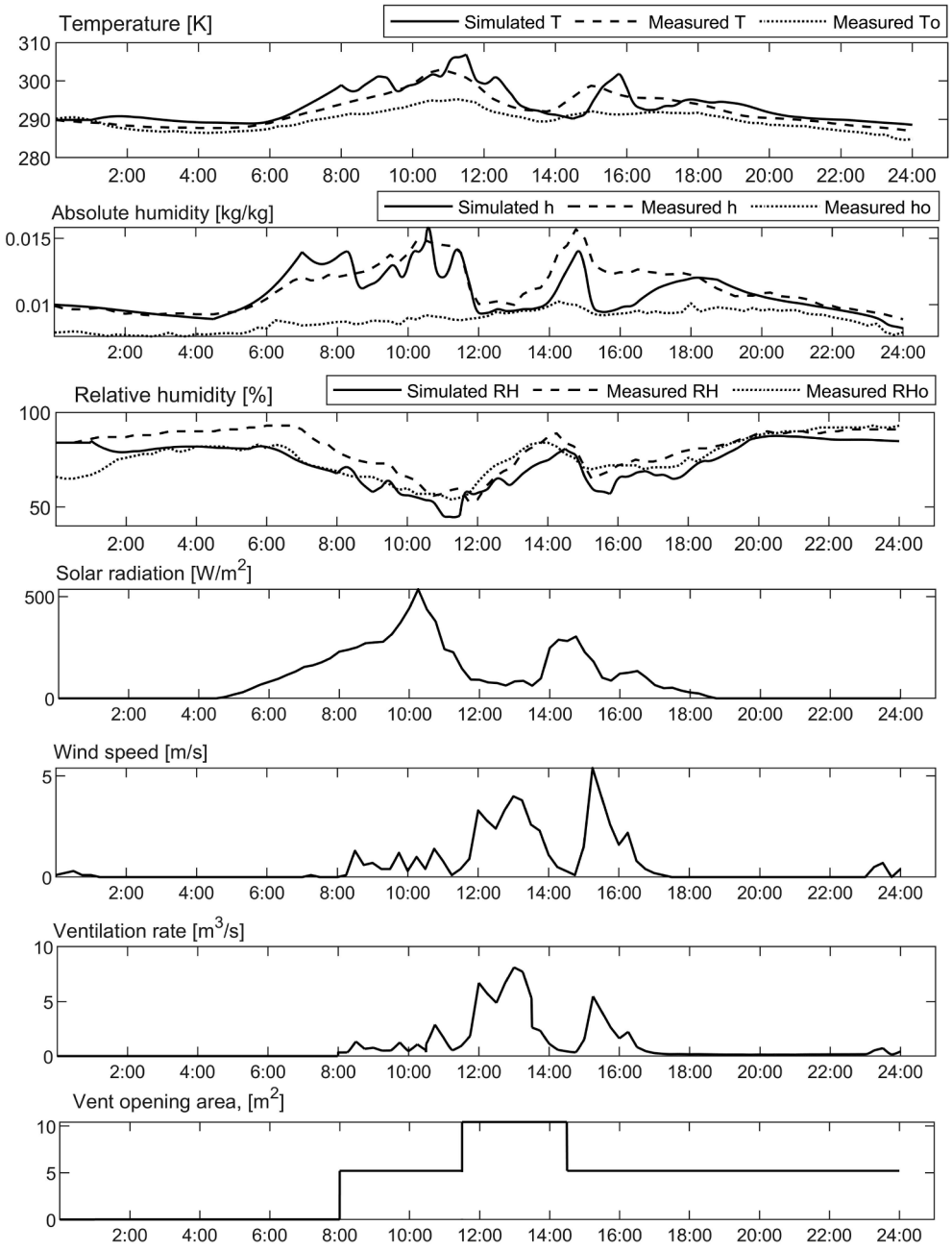

Fig. 10. Data set of the temperature, humidity, outdoor solar radiation, wind speed, simulated ventilation rate and the vent opening area under the single-vent opening configuration on 9 May 2019 in Greenhouse A.

Table 3
The Root Mean Squared Error (RMSE) and Mean Error (ME) of the simulated greenhouse temperature and humidity for each test.

Test	Week	RMSE / ME			Greenhouse
		T (K)	h (g kg^{-1})	RH (%)	
No. 1	20/09/2016–26/09/2016	2.3 / 1.5	1.3 /1.1	11.4 / 8.4	A
No. 2	10/05/2016–16/05/2016	2.8 / 2.0	1.5 / 2.1	16.6 / 13.1	A
No. 3	20/09/2019–26/09/2019	2.0 / 1.6	0.8 / 0.6	8.8 / 6.9	B
No. 4	18/11/2019–24/11/2019	2.8 / 1.9	1.8 / 1.2	11.7 / 9.5	B

model's system is solving the closed-equations group for the wall and roof temperature. Even so, the total running time for a 24 h simulation period is less than 15 mins (using an Intel Core I7 CPU and 16 GB RAM). The model's portability is especially significant, allowing it to be deployed in practical greenhouse cultivation to facilitate future decision-making management and real-time closed-loop automatic control.

Temperature and humidity interact with each other inside a greenhouse via the sensible and latent heat transitions; this makes it difficult to quantify the source term for the energy and water vapor. Therefore, in most of the current studies, black box techniques have been used to develop the greenhouse's temperature and humidity model. The model described in this paper quantified the water–vapor source term by incorporating the phase transition, leaf transpiration, leaf condensation, and the indoor/outdoor humidity exchange, to develop a mechanistic

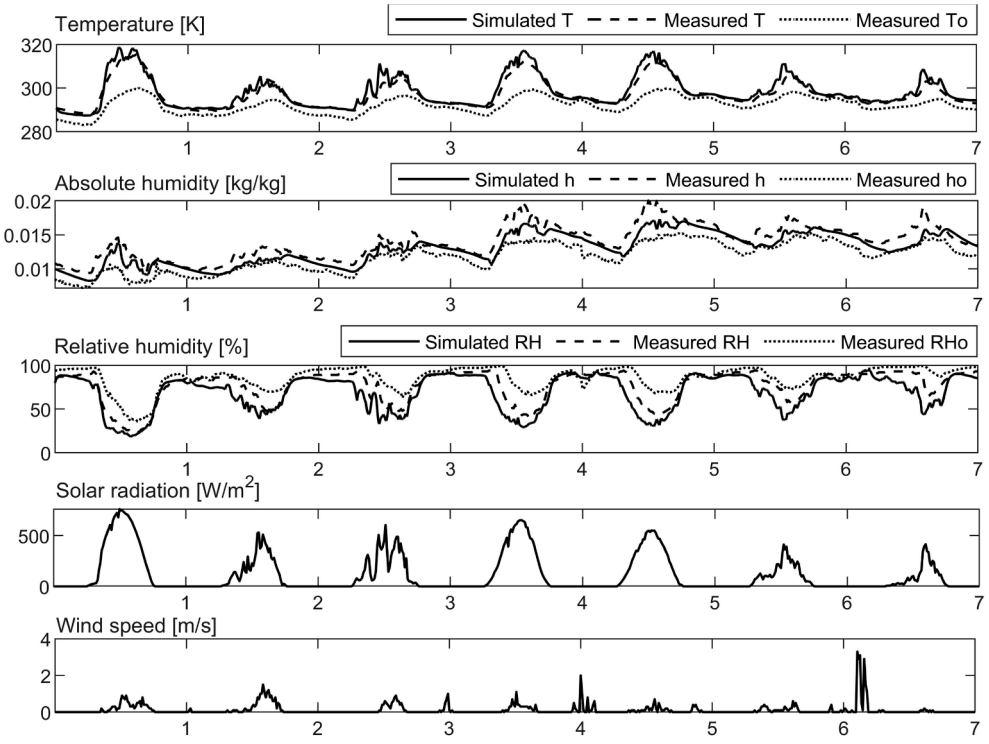

Fig. 11. Data set used for the model validation with the temperature and humidity, recorded on 20–26 September 2016 in Greenhouse A.

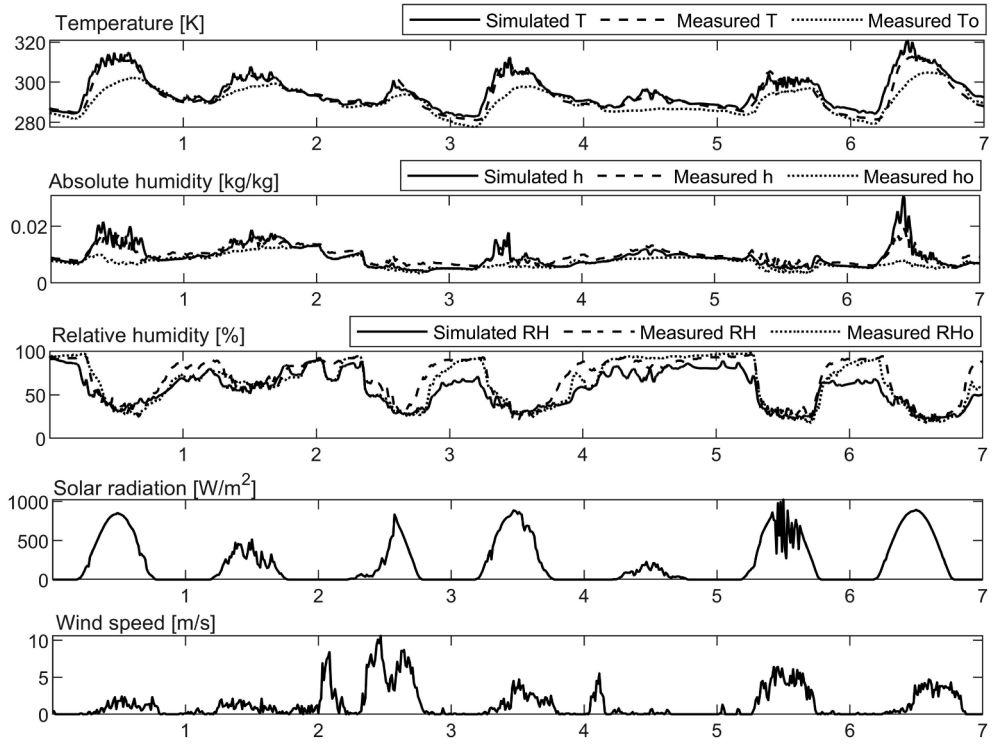

Fig. 12. Data set used for the model validation with the temperature and humidity on 10–16 May 2016 in Greenhouse A.

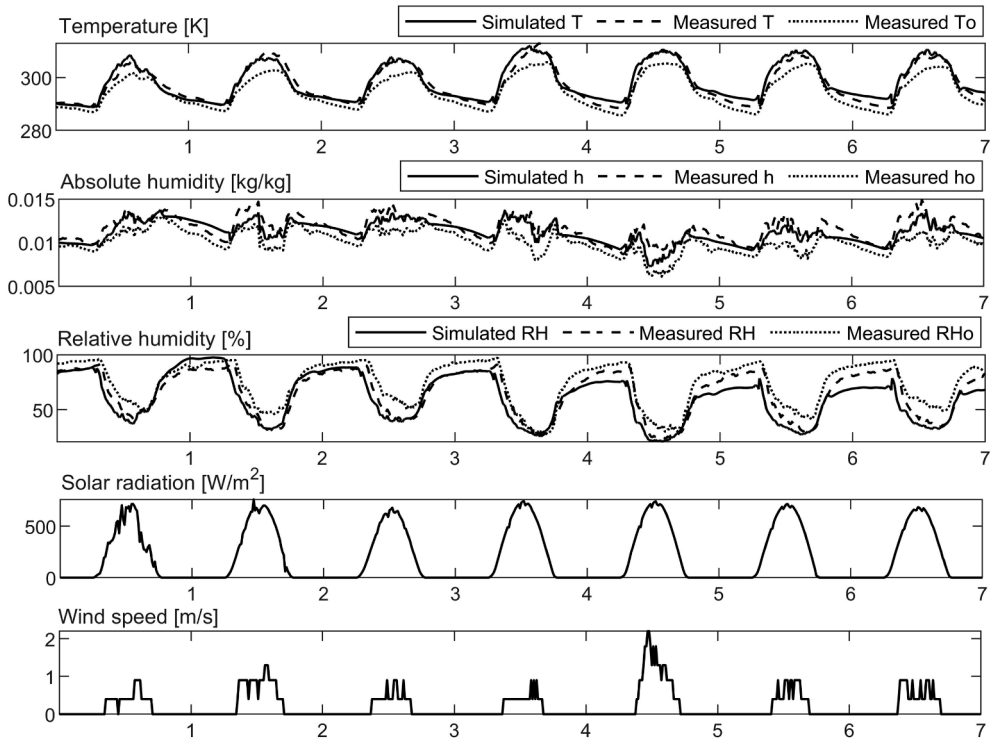

Fig. 13. Data set used for the model validation with the temperature and humidity on 20–26 September 2019 in Greenhouse B.

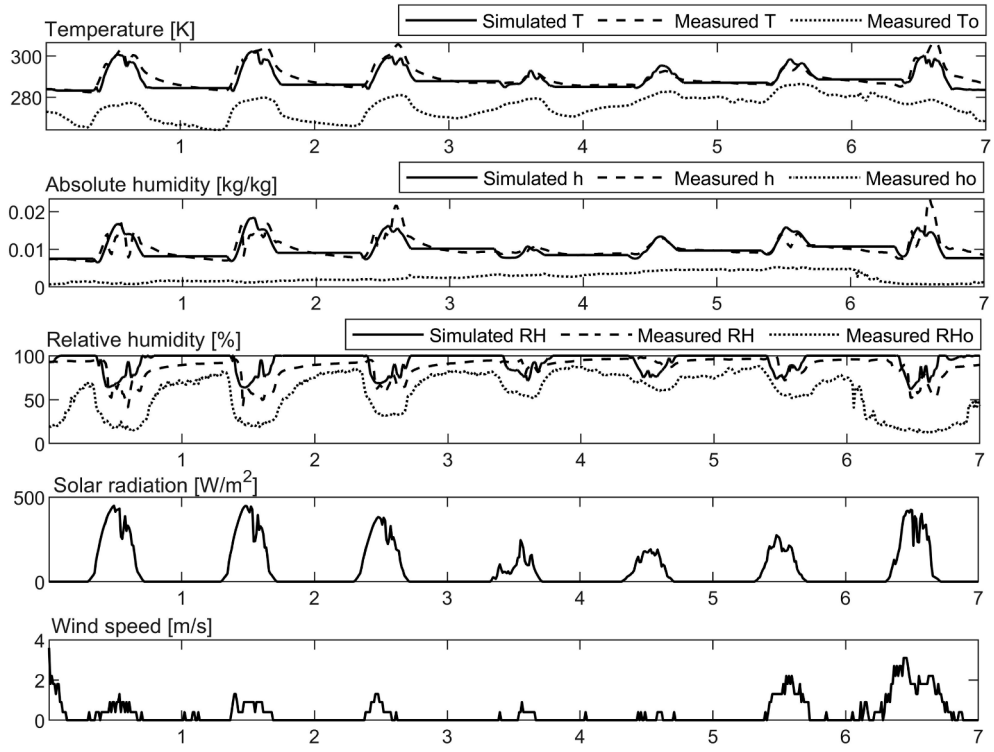

Fig. 14. Data set used for the model validation with the temperature and humidity on 18–24 November 2019 in Greenhouse B; the thermal insulation blanket covering was deployed from 17:00 to 08:00 every day.

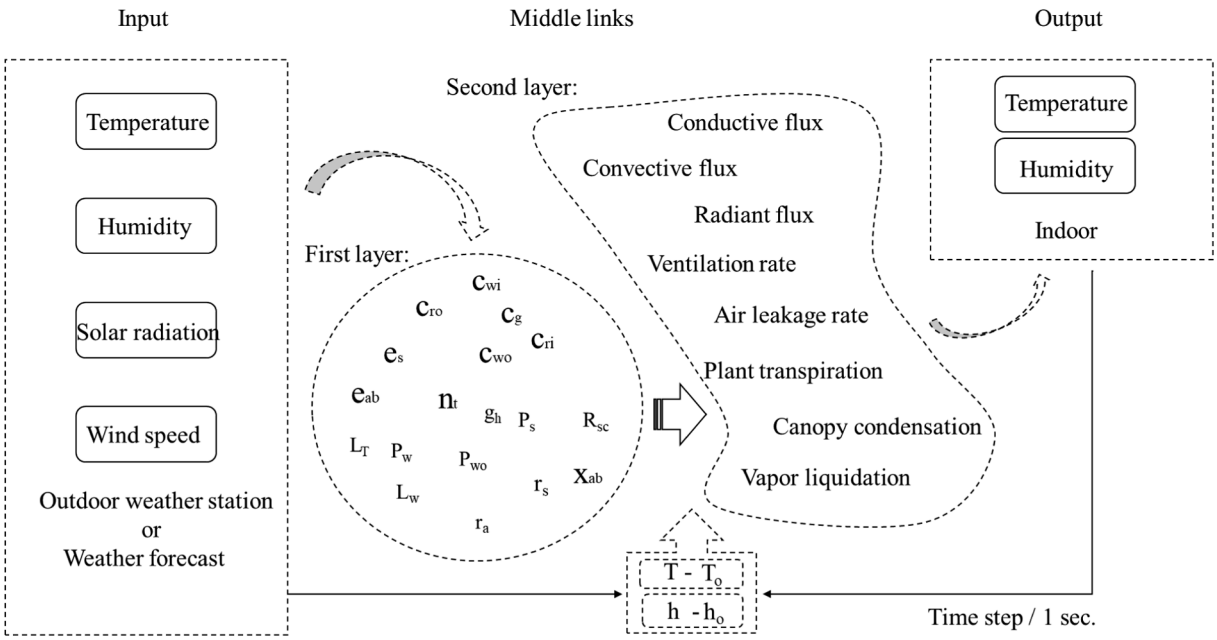

Fig. 15. Inputs, middle links, and outputs of the model. A description of the figure's characters is given in Appendix A.

greenhouse temperature and humidity model, which has been utilized to study Chinese single-slope greenhouses for the first time.

The model developed in this paper is a flexible and valuable tool that can be used for climate simulation, temperature and humidity control, and as decision support tool in Chinese solar greenhouses. Nevertheless, further research need to be undertaken, for example, developing crop models for particular cultivars, models that precisely simulate soil evaporation and ventilation, and optimization between one dimension and multi-dimension models.

Declaration of Competing Interest

The authors declare that they have no known competing financial interests or personal relationships that could have appeared to influence the work reported in this paper.

Acknowledgements

Liu Ran is most grateful for the financial support given by the China Scholarship Council for this research (no. 201909505002). This work has been funded by Project DPI2017-85007-R of the Spanish Ministry of Science, Innovation and Universities, and by ERDF funds.

References

Ahamed, M.S., Guo, H.Q., Tanino, K., 2018. Development of a thermal model for simulation of supplemental heating requirements in Chinese-style solar greenhouses. Computers and Electronics in Agriculture. 150, 235–244. https://doi.org/10.1016/j.compag.2018.04.025.

Ahmed, H.A., TONG, Y.X., YANG, Q.C., Al-Faraj, A.A., Abdel-Ghany, A.M., 2019. Spatial distribution of air temperature and relative humidity in the greenhouse as affected by external shading in arid climates. Journal of Integrative Agriculture. 18 (12), 2869-2882. https://doi.org/10.1016/S2095-3119(19)62598-0.

Boulard, T., Roy, J.C., Fatnassi, H., Kichah, A., Lee, I.-B., 2010. Computer fluid dynamics prediction of climate and fungal spore transfer in a rose greenhouse. Computers and Electronics in Agriculture. 74 (2), 280–292. https://doi.org/10.1016/j.compag.2010.09.003.

Boulard, T., Roy, J.C., Pouillard, J.-B., Fatnassi, H., Grisey, A., 2017. Modelling of micrometeorology, canopy transpiration and photosynthesis in a closed greenhouse using computational fluid dynamics. Biosystems Engineering. 158, 110–133. https://doi.org/10.1016/j.biosystemseng.2017.04.001.

Boulard, T., Wang, S., 2002. Experimental and numerical studies on the heterogeneity of crop transpiration in a plastic tunnel. Computers and Electronics in Agriculture. 34, 173–190. https://doi.org/10.1016/S0168-1699(01)00186-7.

Carlini, M., Castellucci, S., Mennuni, A., Morelli, S., 2020. Numerical modeling and simulation of pitched and curved-roof solar greenhouses provided with internal heating systems for different ambient conditions. Energy Reports. 6 (3), 146–154. https://doi.org/10.1016/j.egyr.2019.10.033.

Chen, J.T., Ma, Y.W., Pang, Z.Z., 2020. A mathematical model of global solar radiation to select the optimal shape and orientation of the greenhouses in southern China. Solar Energy. 205, 380–389. https://doi.org/10.1016/j.solener.2020.05.055.

Choab, N., Allouhi, A., El Maakoul, A., Kousksou, T., Saadeddine, S., Jamil, A., 2019. Review on greenhouse microclimate and application: Design parameters, thermal modeling and simulation, climate controlling technologies. Solar Energy. 191, 109–137. https://doi.org/10.1016/j.solener.2019.08.042.

De Halleux, D., 1989. Dynamic model of heat and mass transfer in greenhouses: theoretical and experimental study. PhD Thesis, Gembloux, Belgium.

Gerlein-Safdi, C., Koohafkan, M.C., Chung, M., Rockwell, F.E., Thompson, S., Caylor, K. K., 2018. Dew deposition suppresses transpiration and carbon uptake in leaves. Agricultural and Forest Meteorology. 259, 305–316. https://doi.org/10.1016/j.agrformet.2018.05.015.

Guo, H.E., Liu, B., Wang, X., Zhang, C.K., 2016. Current situation and countermeasures for the development of the solar greenhouse in Shandong province. Bulletin of Agricultural Science and Technology. 10, 5–8. https://doi.org/10.3969/j.issn.1000-6400.2016.10.001.

He, F., Ma, C.W., 2010. Modeling greenhouse air humidity by means of artificial neural network and principal component analysis. Computers and Electronics in Agriculture. 71. Supplement 1, S19–S23. https://doi.org/10.1016/j.compag.2009.07.011.

Huang, S., Yan, H.F., Zhang, C., Wang, G.Q., Acquah, S.J., Yu, J.J., Li, L.L., Ma, J.M., Darko, R.O., 2020. Modeling evapotranspiration for cucumber plants based on the Shuttleworth-Wallace model in a Venlo-type greenhouse. Agricultural Water Management. 228, 105861 https://doi.org/10.1016/j.agwat.2019.105861.

Jolliet, O., Danloy, L., Gay, J.B., Munday, G.L., Reist, A., 1991. HORTICERN: an improved static model for predicting the energy consumption of a greenhouse. Agricultural and Forest Meteorology. 55 (3–4), 265–294. https://doi.org/10.1016/0168-1923(91)90066-Y.

Jung, D.H., Kim, H.S., Jhin, C., Kim, H.-J., Park, S.H., 2020. Time-serial analysis of deep neural network models for prediction of climatic conditions inside a greenhouse. Computers and Electronics in Agriculture. 173, 105402 https://doi.org/10.1016/j.compag.2020.105402.

Kichah, A., Bournet, P.-E., Migeon, C., Boulard, T., 2012. Measurement and CFD simulation of microclimate characteristics and transpiration of an Impatiens pot plant crop in a greenhouse. Biosystems Engineering. 112, 22–34. https://doi.org/10.1016/j.biosystemseng.2012.01.012.

Kustas, W., Rango, A., Uijlenhoet, R., 1994. A simple energy budget algorithm for the snowmelt runoff model. Water Resources Res. 30, 1515–1527. https://doi.org/10.1029/94WR00152.

Li, K.J., Sha, Z.D., Xue, W.P., Chen, X., Mao, H.P., Tan, G., 2020. A fast modeling and optimization scheme for greenhouse environmental system using proper orthogonal decomposition and multi-objective genetic algorithm. Computers and Electronics in Agriculture. 168, 105096 https://doi.org/10.1016/j.compag.2019.105096.

Li, T.H., Chang, J.M., Wei, M., Shi, G.Y., Zhang, Y.S., Chen, D.J., 2018. Application situation and problem analysis of ventilation facilities in solar greenhouse in Shandong province. Agricultural Engineering and Technology. 38 (16), 22-26. (In Chinese) https://doi.org/10.16815/j.cnki.11-5436/s.2018.16.003.

Liu C.X., Ma C.W., Wang P.Z., Zhao S.M., Cheng J.Y., Wang M.L., 2015. Analysis on affecting factors of heat preservation properties for thermal insulation covers. Transactions of the CSAE. 31 (20), 186-193. (In Chinese) https://doi.org/10.11975/j.issn.1002-6819.2015.20.026.

Liu, H.J., Yin, C.Y., Gao, Z.Z., Hou, L.Z., 2021. Evaluation of the cucumber yield, economic benefit, and water productivity under different soil matric potentials in solar greenhouses in North China. Agricultural Water Management. 243, 106442 https://doi.org/10.1016/j.agwat.2020.106442.

Liu X.Y., Zhang W., 2011. Establishment and analysis of forecasting model of temperature and humidity in PC board greenhouse. Agriculture Network Information. 7, 31-33. (In Chinese) https://kns.cnki.net/kcms/detail/detail.aspx?FileName=JSJN201107010&DbName=CJFQ2011.

Ma C., Wang Lin., Ding X., Hou C., Han J., 2008. Theories and methods for calculation of ventilation rate in design rule for greenhouse ventilation. Journal of Shanghai Jiaotong university (Agricultural Science). 26 (5), 416-423. (In Chinese) http://en.cnki.com.cn/Article_en/CJFDTotal-SHNX200805019.htm.

McClellan, T.M., Pedersen, C.O., 1997. Investigation of outside heat balance models for use in a heat balance cooling load calculation procedure. ASHRAE Transactions. 103 (2), 469–484.

Medrano, E., Lorenzo, P., Sánchez-Guerrero, M.C., Montero, J.I., 2005. Evaluation and modelling of greenhouse cucumber-crop transpiration under high and low radiation conditions. Scientia Horticulturae 105 (2), 163–175. https://doi.org/10.1016/j.scienta.2005.01.024.

Mirsadeghi, M., Cóstola, D., Blocken, B., Hensen, J.L.M., 2013. Review of external convective heat transfer coefficient models in building energy simulation programs: Implementation and uncertainty. Applied Thermal Engineering. 56 (1–2), 134–151. https://doi.org/10.1016/j.applthermaleng.2013.03.003.

Modest, M.F., 1993. Radiative Heat Transfer. McGraw-Hill, New York https://www.sciencedirect.com/book/9780123869449/radiative-heat-transfer.

Mohammadi, B., Ranjbar, S.F., Ajabshirchi, Y., 2018. Application of a dynamic model to predict some inside environment variables in a semi-solar greenhouse. Information Processing in Agriculture. 5 (2), 279–288. https://doi.org/10.1016/j.inpa.2018.01.001.

NY/T 1451-2018, 2018. Code for ventilation design of greenhouse. Ministry of Agriculture of the PRC. P:7-8. (In Chinese).

Papadakis, G., Frangoudakis, A., Kyritsis, S., 1992. Mixed, forced, and free convection heat transfer at the greenhouse cover. Journal of Agricultural Engineering Research. 51, 191–205. https://doi.org/10.1016/0021-8634(92)80037-S.

Righini, I., Vanthoor, B., Verheul, M.J., Naseer, M., Maessen, H., Persson, T., Stanghellini, C., 2020. A greenhouse climate-yield model focussing on additional light, heat harvesting and its validation. Biosystems Engineering. 194, 1–15. https://doi.org/10.1016/j.biosystemseng.2020.03.009.

Rodriguez, F., Berenguel, M., Guzman, J.L., Ramirez-Arias, A., 2015. Modeling and control of greenhouse crop growth. Advances in Industrial Control. https://doi.org/10.1007/978-3-319-11134-6.

Roy, J.C., Boulard, T., Kittas, C., Wang, S., 2002. PA—Precision Agriculture: Convective and Ventilation Transfers in Greenhouses, Part 1: The Greenhouse considered as a Perfectly Stirred Tank. Biosystems Engineering. 83 (1), 1–20. https://doi.org/10.1006/bioe.2002.0107.

Sánchez-Molina, J., Li, M., Rodriguez, F., Guzmán, J., Wang, H., Yang, X., 2017. Development and test verification of an air temperature model for Chinese solar and Spanish Almeria-type greenhouse. International Journal of Agricultural and Biological Engineering. 10, 66–76. https://doi.org/10.25165/j.ijabe.20171004.2398.

Singh, G., Singh, P.P., Singh Lubana, P.P., Singh, K.G., 2006. Formulation and validation of a mathematical model of the microclimate of a greenhouse. Renewable Energy. 31 (10), 1541–1560. https://doi.org/10.1016/j.renene.2005.07.011.

Snyder, R.L., Shaw, R.H., 1984. Converting humidity expressions with computers and calculators. University of California, Division of Agriculture and Natural Resources.

Soriano, T., Montero, J.I., Sánchez-Guerrero, M.C., Medrano, E., Antón, A., Hernández, J., Morales, M.I., Castilla, N., 2004. A Study of Direct Solar Radiation Transmission in Asymmetrical Multi-span Greenhouses using Scale Models and Simulation Models. Biosystems Engineering. 88 (2), 243–253. https://doi.org/10.1016/j.biosystemseng.2004.03.006.

Sparrow, E.M., Ramsey, J.W., Mass, E.A., 1979. Effect of Finite Width on Heat Transfer and Fluid Flow about an Inclined Rectangular Plate. Journal of Heat Transfer. 101, 199–204. https://doi.org/10.1115/1.3450946.

Tong, G.H, Che, Z.S., Bai, Y.K., Yamaguchi, T., 2008. Air exchange rate calculation for solar greenhouse using thermal balance method. Journal of Shenyang Agricultural University. 39 (4), 459-462. (In Chinese) https://doi.org/10.3969/j.issn.1000-1700.2008.04.017.

Tong, G.H., Christopher, D.M., Li, B., 2009. Numerical modelling of temperature variations in a Chinese solar greenhouse. Computers and Electronics in Agriculture. 68 (1), 129–139. https://doi.org/10.1016/j.compag.2009.05.004.

Tong G.H., Li B.M., Christopher D.M., Yamaguchi T., 2007. Preliminary study on temperature pattern in a Chinese solar greenhouse using computational fluid dynamic. Transactions of the CSAE. 23 (7), 178-185. (In Chinese) https://doi.org/10.3321/j.issn:1002-6819.2007.07.035.

Villarreal-Guerrero, F., Kacira, M., Fitz-Rodríguez, E., Kubota, C., Giacomelli, G.A., Linker, R., Arbel, A., 2012. Comparison of three evapotranspiration models for a greenhouse cooling strategy with natural ventilation and variable high-pressure fogging. Scientia Horticulturae. 134, 210–221. https://doi.org/10.1016/j.scienta.2011.10.016.

Walton, G.N., 1981. Passive Solar Extension of the Building Loads Analysis and System Thermodynamics (BLAST) Program. United States Army Construction Engineering Research Laboratory, Champaign, IL.

Walton, G.N., 1983. Thermal Analysis Research Program Reference Manual, NBSSIR 83–2655. National Bureau of Standards.

Wen, D., Wang, X., Sun, K.N., Wang, K.A., Yang, N., 2019. Development situation and prospects of mechanization for greenhouse vegetables in Shandong province. Agricultural Equipment & Vehicle Engineering. 57 (S1), 52-54. (In Chinese) https://doi.org/10.3969/j.issn.1673-3142.2019.S1.012.

Zhang, G.S., Ding, X.M., Li, T.H., Pu, W.Y., Lou, W., Hou, J.L., 2020a. Dynamic energy balance model of a glass greenhouse: An experimental validation and solar energy analysis. Energy. 198, 117281 https://doi.org/10.1016/j.energy.2020.117281.

Zhang, G.X., Fu, Z.T., Yang, M.S., Liu, X.X., Dong, Y.H., Li, X.X., 2019a. Nonlinear simulation for coupling modeling of air humidity and vent opening in Chinese solar greenhouse based on CFD. Computers and Electronics in Agriculture. 162, 337–347. https://doi.org/10.1016/j.compag.2019.04.024.

Zhang, X.D., Lv, J., Dawuda, M.M., Xie, J.M., Yu, J.H., Gan, Y.T., Zhang, J., Tang, Z.Q., Li, J., 2019b. Innovative passive heat-storage walls improve thermal performance and energy efficiency in Chinese solar greenhouses for non-arable lands. Solar Energy. 190, 561–575. https://doi.org/10.1016/j.solener.2019.08.056.

Zhang, Y., Henke, M., Li, Y.M., Yue, X., Xu, D.M., Liu, X.G., Li, T.L., 2020b. High resolution 3D simulation of light climate and thermal performance of a solar greenhouse model under tomato canopy structure. Renew. Energy 160, 730–745. https://doi.org/10.1016/j.renene.2020.06.144.

Zhao, C.J., Li, M., Yang, X.T., Sun, C.H., Qian, J.P., Ji, Z.T., 2011. A data-driven model simulating primary infection probabilities of cucumber downy mildew for use in early warning systems in solar greenhouses. Computers and Electronics in Agriculture. 76 (2), 306–315. https://doi.org/10.1016/j.compag.2011.02.009.

Zou, W.D., Yao, F.X., Zhang, B.H., He, C.X., Guan, Z.X., 2017. Verification and predicting temperature and humidity in a solar greenhouse based on convex bidirectional extreme learning machine algorithm. Neurocomputing. 249, 72–85. https://doi.org/10.1016/j.neucom.2017.03.023.